ISPRS Journal of Photogrammetry and Remote Sensing xxx (2017) xxx–xxx

Contents lists available at ScienceDirect

ISPRS Journal of Photogrammetry and Remote Sensing

journal homepage: www.elsevier.com/locate/isprsjprs

Lightweight UAV with on-board photogrammetry and single-frequency GPS positioning for metrology applications

M. Daakir [a,c,*], M. Pierrot-Deseilligny [c], P. Bosser [b], F. Pichard [a], C. Thom [c], Y. Rabot [a], O. Martin [c]

[a] Vinci-Construction-Terrassement/Sixense Mapping, 1, Rue du docteur Charcot, 91421 Morangis, France
[b] ENSTA Bretagne-OSM Team, 2 rue Francois Verny, 29806 Brest, France
[c] Université Paris-Est, IGN, LaSTIG, LOEMI, 73 avenue de Paris, 94160 Saint-Mandé, France

ARTICLE INFO

Article history:
Received 14 February 2016
Received in revised form 10 December 2016
Accepted 18 December 2016
Available online xxxx

Keywords:
UAV
GPS
Photogrammetry
ISO
Metrology
Lever-arm

ABSTRACT

This article presents a coupled system consisting of a single-frequency GPS receiver and a light photogrammetric quality camera embedded in an Unmanned Aerial Vehicle (UAV). The aim is to produce high quality data that can be used in metrology applications. The issue of Integrated Sensor Orientation (ISO) of camera poses using only GPS measurements is presented and discussed. The accuracy reached by our system based on sensors developed at the French Mapping Agency (*IGN*) Opto-Electronics, Instrumentation and Metrology Laboratory (*LOEMI*) is qualified. These sensors are specially designed for close-range aerial image acquisition with a UAV. Lever-arm calibration and time synchronization are explained and performed to reach maximum accuracy. All processing steps are detailed from data acquisition to quality control of final products. We show that an accuracy of a few centimeters can be reached with this system which uses low-cost UAV and GPS module coupled with the *IGN-LOEMI* home-made camera.

1. Introduction

Nowadays, a lot of applications use UAVs. The field of aerial photography is one of the areas where the activities of civilian UAVs are the most important. Close-range aerial photogrammetry is positioned as a leading application for the use of aerial photography for mapping purposes, inspection, metrology, etc. The primary purpose of photogrammetry is to describe the geometry of a scene with high fidelity. Generally, during photogrammetric data processing, after estimating camera poses, the conversion of these poses in an absolute frame is essential to express the results in a legal metric system. This step may be carried out conventionally by providing targets on the scene that was captured and which have been measured by surveying for instance. This method is more commonly known as indirect-georeferencing. Another method used to achieve the same step and which reduces significantly the working time spent in the field is to couple the embedded camera with a GNSS/INS sensors (Skaloud, 2002). In this way, the image position and the image orientation are directly expressed into the absolute frame. In this article we present a coupled system composed of a camera and a GPS module allowing to achieve integrated sensor orientation of aerial images performed by a UAV. This article shows one of the possible fields of application of the home-made *IGN LOEMI* laboratory sensors. Also, it presents the first photogrammetric results obtained with the light UAV-metric camera whose hardware development began in 2012. Section 2 presents a brief review of researches that have been conducted recently in this area particularly since the use of UAVs was generalized. Section 3 will give the characteristics of the sensors used in our study. Section 4 describes the data processing strategy adopted and explains the steps to perform geometrical calibration of the instruments and the importance of sensors time synchronization. Finally, Section 5 will give the results obtained following an experiment carried out using our UAV on-board system.

* Corresponding author at: Université Paris-Est, IGN, SRIG, LOEMI, 73 avenue de Paris, 94160 Saint-Mandé, France.
E-mail addresses: mehdi.daakir@vinci-construction.com (M. Daakir), marc.pierrot-deseilligny@ensg.eu (M. Pierrot-Deseilligny), pierre.bosser@ensta-bretagne.fr (P. Bosser), francis.pichard@vinci-construction.com (F. Pichard), christian.thom@ign.fr (C. Thom), yohann.rabot@vinci-construction.com (Y. Rabot), olivier.martin@ign.fr (O. Martin).

http://dx.doi.org/10.1016/j.isprsjprs.2016.12.007
0924-2716/

2. UAV literature review

For over a decade, we have been witnessing an evolution in the development of UAV systems. These systems are increasingly miniaturized, lightweight, and carry various of sensors. These systems have a high potential especially as the fields of application are diverse: agriculture (Grenzdörffer et al., 2008), forestry (Lisein et al., 2013), cultural heritage (Eisenbeiß, 2004), mapping and 3D modeling (Remondino et al., 2011) also dedicated to archaeology, metrology and monitoring (Tournadre et al., 2014), geology (Niethammer et al., 2012), etc. Moreover, regulation of air space evolves and give to these airborne systems the opportunity to grow in the context of a clear regulatory framework.

UAV photogrammetry (Eisenbeiß, 2009) takes advantage of this trend to establish itself as an essential application of aerial photography today (Colomina and Molina, 2014). One of the limitations that arises when dealing with photogrammetric data processing is the georeferencing part to express results in an absolute system. A conventional method used in aerial photogrammetry is to have targets on the scene whose coordinates are measured by surveying, which are then used to convert the cameras poses from relative into absolute system. This technique is very effective but has some drawbacks: the establishment and measurement of targets network is time consuming or sometimes the scene ahead is inaccessible and does not allow secure access. This is why, this technique is very restrictive in the context of large aerial surfaces acquisitions.

The real-time positioning for absolute georeferencing purpose is a problem widely studied. It is possible to achieve a centimeter positioning accuracy (Eling et al., 2015) which will allow to convert the camera poses in an absolute reference system. In the context of on-board UAV photogrammetry, these solutions are generally heavy and based on dual-frequency GNSS receivers whose price today is still relatively significant (Rehak et al., 2013; Rieke et al., 2011) and achieve a typical absolute georeferencing accuracy of 1–5 cm with the use of 0 or 1 ground control point. Other research focuses on the "low-cost" aspect of on-board sensors and platform used (Bendea et al., 2008; Bláha et al., 2011; Chiang et al., 2012; Stempfhuber and Buchholz, 2011). These solutions are generally based on single-frequency GPS receivers whose data are certainly sufficient for navigation, but the accuracy of positioning remains metric. We want to show in this paper that with a UAV equipped with a single-frequency GPS receiver it is possible to achieve an absolute accuracy of 1–3 cm. To achieve this accuracy, it is essential to follow a strict processing data protocol and a rigorous preliminary calibration phase discussed in the following.

3. Hardware

Here, we give details on the sensors used in our experiment. These sensors are entirely developed internally within the laboratory. The UAV is an entry-level model available on the market as an assembly kit or RTF[1] format. Furthermore, one of our purposes is to achieve a light system performing accurate absolute georeferencing without exceeding 2 kg for law restrictions from a point of view of the regulations that governed evolution of UAVs in the French airspace.

3.1. Camera

The on-board camera (Martin et al., 2014) is a home-made camera specially designed for close-range photogrammetric UAV acquisitions (Fig. 1). This camera has the advantage of being low-mass, 300 g including the lens. The imaging sensor chosen is a full frame *CMOS* of 20 Mpx. Another advantage is the modular aspect of the camera that makes it possible, for instance, to integrate a GPS chip within the same enclosure. Besides, this camera has the ability to acquire images at a very high rate, up to 4 frames per second at full resolution and save in a non-degraded raw format. This will be the case for the next version (1.1) of the camera, currently in testing phase. The version used here allows for now to acquire images at a frequency of 0.5 Hz. Next, the camera has photogrammetric properties: used only with a fixed focal lens length, a global shutter to avoid tearing effects seen with rolling shutters due to UAV movements and a high geometric stability has been verified on various acquisitions made during the same day.

Fig. 1. IGN light camera dedicated to photogrammetric UAV applications.

Another important aspect, which will be detailed in Section 4.5, is the fact that the camera has been developed with a strong constraint on the ability of offering a stable time synchronization. This allows us to neglect error residual due to electronic delay between GPS receiver observations and triggering images by the camera.

3.2. GPS chip

The GPS module chosen is the one used by the *GeoCube*, a multi-sensor geo-monitoring system developed at the *IGN LOEMI* laboratory (Fig. 2). The *GeoCube* was initially developed for deformation monitoring applications (Benoit et al., 2015) over long periods of static observation sessions. In this study, the *GeoCube* is used in a kinematic configuration. The integrated GPS chip is the *u-blox* LEA-6T-0-001 model (u-blox, 2015). It records raw C/A[2] code, carrier-phase and Doppler data of GPS satellites constellation on GPS L1[3] band. Post-processing of recorded data makes it possible, for short baselines, to get an accurate relative positioning with respect to a known reference station.

The first benefit of this *u-blox* GPS module is its price. It costs less than €100. In our configuration, it is used with a *Taoglas* brand patch antenna. In addition, this GPS module offers some useful features for time synchronization with the camera. The *TimePulse* (u-blox, 2013) feature allows to send a PPS[4] in a synchronized way in GPS time-scale with an accuracy of 30 ns RMS.[5] The *TimeMark* (u-blox, 2013) is used to date events in the GPS time-scale. All these features can be easily activated and set up using *u-center* (u-blox, 2016) software provided by *u-blox* company.

[1] Ready to Fly.

[2] Coarse/Acquisition.

[3] 1575.42 MHz.

[4] Pulse Per Second.

[5] Root Mean Square.

Please cite this article in press as: Daakir, M., et al. Lightweight UAV with on-board photogrammetry and single-frequency GPS positioning for metrology applications. ISPRS J. Photogram. Remote Sensing (2017), http://dx.doi.org/10.1016/j.isprsjprs.2016.12.007

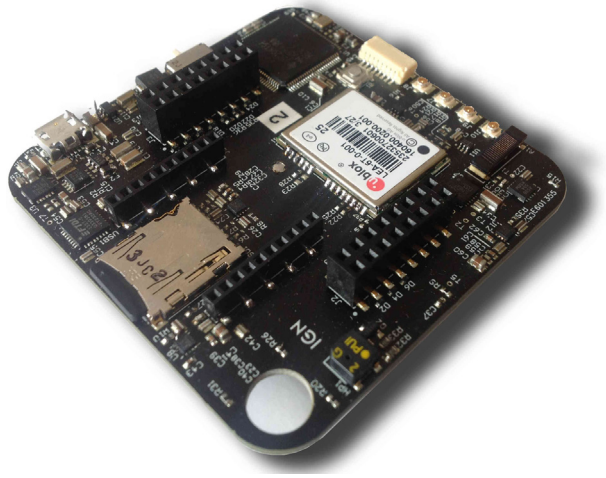

Fig. 2. IGN GeoCube module with an u-blox GPS chip.

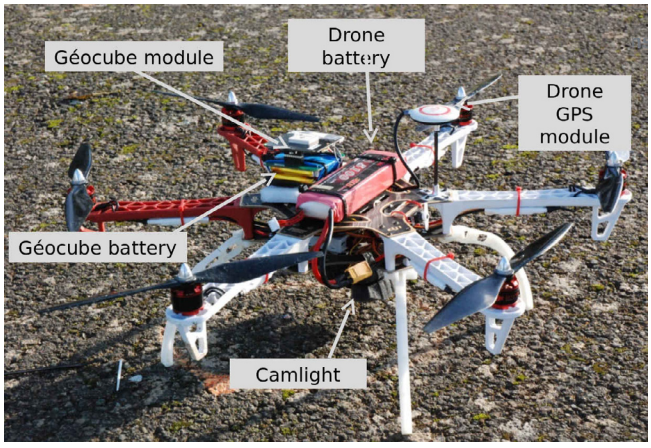

Fig. 3. UAV prototype developed during our work.

3.3. UAV

The UAV used in our experiments is the F-550 (DJI Innovations, 2015a) model developed by *DJI* (Fig. 3). This UAV is a hexacopter type which allows a more stabilized flight, making it a good choice for aerial photography. This UAV uses the *WOOKONG-M* (DJI Innovations, 2014) autopilot also developed by *DJI*. This system offers a flight control software, *DJI Ground Station* (DJI Innovations, 2015b), to allow performing acquisitions in automatic mode. One disadvantage of this model is its flying range that remains below 15 min. However, this UAV can take-off with a payload capacity of only 2 kg. It is very affordable: the pre-assembled copter costs less than €500 online.

4. Data processing

To achieve integrated sensor orientation of a photogrammetric acquisition based on GPS on-board observations, we may follow the following procedure:

- process relative camera poses based on tie points (Section 4.1),
- compute precise GPS trajectory based on carrier-phase measurements (Section 4.2),
- match camera centers with GPS positions (Section 4.3),
- perform precise lever-arm calibration (Section 4.4),
- achieve time synchronization between the two sensors (Section 4.5),
- perform sensors data fusion using all available measurements (Section 4.6).

4.1. Bundle block adjustment

The estimation of camera poses is performed using the free open source software *Apero-MicMac* (Pierrot-Deseilligny and Clery, 2011) developed by *IGN*. This software is particular by the sense that it offers a fine setting for each step of a photogrammetric processing. This advantage makes it a very powerful tool but a very complex one to handle too. *APERO* uses an implementation of *SIFT* (Lowe, 2004) algorithm for tie points extraction from pairs of images. Based on tie points, it computes relative camera poses based on Bundle Block Adjustment technique (Triggs et al., 1999). *APERO* offers the possibility to estimate intrinsic camera parameters using self-calibration method (Fraser, 1997). Several distortion models are included in *APERO* with more or less degrees of freedom. Some models are physical descriptions of the camera while other models are purely mathematical. All theoretical and practical aspects concerning *APERO* are available in (Pierrot-Deseilligny, 2017).

A critical point in close-range aerial photogrammetry configurations is the estimation of internal parameters by self-calibration technique. With multiple recent studies on the processing of UAV embedded data, the geometric configuration of acquisitions puts forward the drift effect of poses estimation also known as the *bowl effect*, resulting in inaccurate estimates of internal parameters in the bundle block adjustment (James and Robson, 2014; Wu, 2014). A strategy, as given in Tournadre et al. (2015), minimizes this effect by combining two kinds of distortion models: a radial and a non radial one. This strategy can be described by the following steps:

1. initialize a simple camera model from a sub-set of images,
2. use this camera model to estimate all poses,
3. use a physical camera model with more parameters and estimates poses in a self-calibration method,
4. lock the physical camera model and add a polynomial model.

The expression of the system of equations to minimize during the bundle block adjustment can be expressed as follows:

$$\begin{cases} \cdots\cdots \\ \vec{p}_i|_k - \zeta(\pi(\mathcal{R}_k(\vec{P}_i - \vec{C}_k))) = \vec{0} \\ \cdots\cdots \end{cases} \quad (1)$$

where

$\vec{p}_i|_k$ vector of 2d image coordinates of tie point i on image k;
ζ is a $\mathbb{R}^2 \rightarrow \mathbb{R}^2$ application describing the camera model;
π is a $\mathbb{R}^3 \rightarrow \mathbb{R}^2$ projective application;
$(\vec{C}_k, \mathcal{R}_k)$ position and orientation of image k;
$\vec{P}_i$ vector of 3d position of tie point i.

The processing strategy results in the expression of $\zeta(x,y)$ composed of two applications $\zeta_1 \circ \zeta_2(x,y)$ where ζ_1 describes the physical part of the camera model including a high degrees radial polynomial δr and ζ_2 a lower polynomial degrees δp for the non-radial residual errors remaining whose expressions are:

$$\delta r = \sum_{i=1}^{i=7} a_{2i+1} r^{2i+1} \quad (2)$$

$$\delta p(x,y) = \sum_{i=1}^{i=7}\sum_{j=1}^{j=7} a_{ij} x^i y^j \quad (3)$$

Please cite this article in press as: Daakir, M., et al. Lightweight UAV with on-board photogrammetry and single-frequency GPS positioning for metrology applications. ISPRS J. Photogram. Remote Sensing (2017), http://dx.doi.org/10.1016/j.isprsjprs.2016.12.007

In conventional aerial photogrammetry, it is very common to estimate 3 parameters for the radial polynomial function used to correct the distortion (r^3, r^5, r^7). This was justified by the use of aerial camera with high professional quality optics and also because of the risk of over-parametrization which is considerable with the low number of manual image measurements. Nowadays, on one hand the risk of over-parametrization with the use of high degree polynomial disappear due to adjustment on thousands of tie points per image resulting from automatic algorithm. On the other hand, using standard optics with complex aspheric lenses and relatively high distortion, cannot be modeled with low degree model. Experiment shows that the use of a high degree radial polynomial combined with a lower degree non-radial polynomial improves the accuracy of internal parameters estimation during bundle block adjustment self-calibration (Tang, 2013).

4.2. GPS processing

As for all GNSS data processing, the most important part is fixing to integer values phase ambiguities parameters. In our case, we have to deal with two constraints: a single-frequency GPS receiver and a low number of recorded observations. In fact, this GPS chip records raw carrier-phase measurements only on the first GPS band frequency. As a consequence, the baselines between the reference station and the mobile antenna are limited. A combination of frequencies of the type "iono-free" combination which eliminates the ionospheric delay of the first order cannot be used. Here, the ionospheric delay is estimated with Klobuchar ionospheric model (Klobuchar, 1987) while tropospheric signal delay is corrected using Saastamoinen model (Saastamoinen, 1972). However, given the short baselines we have in our flights configurations, atmospheric delays being spatially correlated, they are eliminated by differentiation of observations between the station and the rover. Beyond the influence of atmospheric errors which are eliminated, the tracking of the signal is of great importance. During the first experiments, a strong instability due to temperature variations was noticed. Indeed, the GPS receiver was not protected and its internal clock showed a large drift because of the ambient temperature variations (Benoit, 2014). This problem is solved by putting the receiver in a waterproof box. Also, the manufacturer allows the configuration of the module according to the dynamics of the platform used, up to accelerations less than 4 g, in order to guarantee the quality of the recorded data.

Observations recorded do not generally exceed 15 min for a sampling frequency of 1 Hz, which does not allow correct estimation of the phase ambiguities as parameters of the problem. The computation strategy adopted is called "fix-and-hold" (Benoit, 2014). The ambiguities are first fixed before UAV take-off. Next, the signal is tracked to detect possible cycle-slips for each satellite observed. With this technique being used, the unknowns yet to estimate are the unknowns of the receiver's position at each epoch. Fig. 4 shows GPS carrier-phase double-difference geometry between a known reference station coordinates and on-board antenna phase center GPS at epoch t_k.

The system of equations of double-difference between 2 satellites and 2 receivers expressed in ECEF[6] reference frame at an epoch t_k can be written as follows:

$$\begin{cases} \vdots \\ \nabla\Delta\left(\Phi_{r_i,r_k}^{s_j,s_l}\right) = \nabla\Delta\left(\rho_{r_i,r_k}^{s_j,s_l}\right) - \lambda_1 \cdot \nabla\Delta\left(N_{r_i,r_k}^{s_j,s_l}\right) \\ -\nabla\Delta\left(\tau_{r_i,r_k,iono}^{s_j,s_l}\right) - \nabla\Delta\left(\tau_{r_i,r_k,tropo}^{s_j,s_l}\right) - \nabla\Delta(\epsilon) \\ \vdots \end{cases} \tag{4}$$

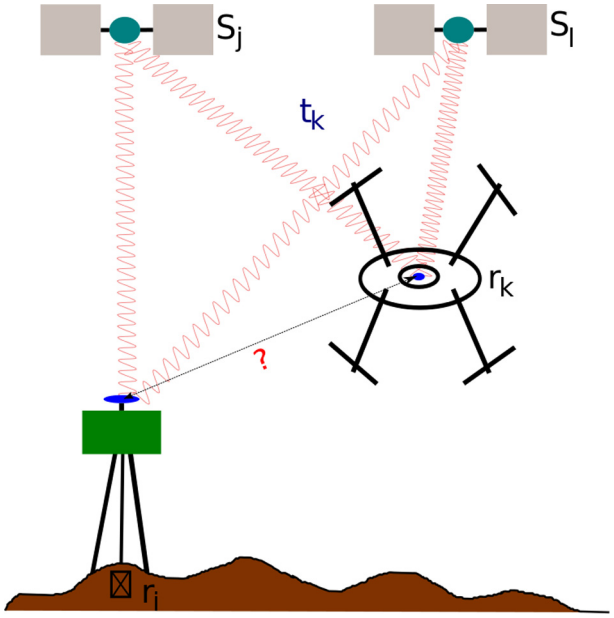

Fig. 4. The double-difference geometry at a single epoch t_k.

where

$\nabla\Delta$ = double-difference operator;
$\Phi_{r_1,r_2}^{s_1,s_2}$ = carrier-phase measurements;
$\rho_{r_1,r_2}^{s_1,s_2}$ = geometric distances;
λ_1 = wavelength of GPS first frequency ($\lambda_1 = 19.03$ cm);
$N_{r_1,r_2}^{s_1,s_2}$ = term of ambiguities;
$\tau_{r_1,r_2,iono}^{s_1,s_2}$ = ionospheric bias;
$\tau_{r_1,r_2,tropo}^{s_1,s_2}$ = tropospheric bias;
ϵ = multipath effect and measurement noise.

If at the first epoch t_0, before UAV take-off, an approximate position of our GPS receiver is given with an accuracy higher than $\lambda_1/2 \approx 10$ cm the term of double-difference of ambiguities can simply be calculated instead of being estimated using (5):

$$\begin{cases} \vdots \\ \nabla\Delta N_{r_i,r_k}^{s_j,s_l} = \left\lfloor \frac{1}{\lambda_1} \cdot \left(\nabla\Delta\left(\Phi_{r_i,r_k}^{s_j,s_l}\right) - \nabla\Delta\left(\rho_{r_i,r_k}^{s_j,s_l}\right)\right. \right. \\ \left. \left. -\nabla\Delta\left(\tau_{r_i,r_k,iono}^{s_j,s_l}\right) - \nabla\Delta\left(\tau_{r_i,r_k,tropo}^{s_j,s_l}\right)\right)\right\rfloor \\ \vdots \end{cases} \tag{5}$$

where $\lfloor\ \rfloor$ = nearest integer operator.

The remaining parameters to estimate in (4) are the axial components of the baseline between the reference station and the mobile antenna at each epoch. These parameters are included in double-difference geometric distances terms.

4.3. GPS positions & camera centers matching

When data acquisition with two different sensors is performed, it is common that the sampling frequencies are not equal. For aerial photogrammetric acquisitions, the maximum flight height allowed, longitudinal and lateral overlap values and the desired GSD[7] will impose the number of images and thus the optimal frame rate. In general, for a UAV acquisition, typical values vary in the range of an image every 2–5 s. On the other hand, the typical sampling frequency for GPS positioning is 1 Hz. So, there are 2–5 times more GPS positions than images acquired, including GPS data

[6] Earth-Centred Earth-Fixed.

[7] Ground Sampling Distance.

Please cite this article in press as: Daakir, M., et al. Lightweight UAV with on-board photogrammetry and single-frequency GPS positioning for metrology applications. ISPRS J. Photogram. Remote Sensing (2017), http://dx.doi.org/10.1016/j.isprsjprs.2016.12.007

recorded during UAV take-off and landing. Fig. 5 shows the result after processing both trajectories in their respective frames.

A common technique to identify corresponding GPS positions to camera centers is Geotagging images with approximate GPS positions determined on flight and in general based on C/A code observations. It is also possible to synchronize the internal clock of the camera with respect to the GPS time-scale. This second solution may be valid only if the internal clock of the camera is stable and does not drift. Another way is to date the triggering of the camera in the GPS time-scale. In our case the camera has no internal clock and the system offers no possibility of Geotagging images.

After performing steps (Sections 4.1 and 4.2), one has 2 trajectories expressed in different frames with different sampling. This technique of centers matching may be useful for users of commercial cameras who cannot perform easily camera clock synchronization or images Geotagging. It may also be useful in the case where the interpolation of image position is not desired. Finally, it can also be used when the electronic delay of the camera is negligible and the triggering of the images is aligned with the GPS TOW[8] for better synchronization accuracy. However a constraint requires that the frequency is supposed to be constant for the entire duration of the acquisition. In this case, it is possible to identify the corresponding positions by computing all possible reasonable[9] combinations for all possible time offsets of successive ratios distances between images centers and a combination of GPS positions.

If a vector v contains n positions as $v = [\vec{P}_1, \ldots, \vec{P}_n]$, the vector v' of successives ratios distances will have $(n-1)$ size as $v' = [r_1, \ldots, r_{n-1}]$, where

$\vec{P}_i$ = camera center of image i;

$r_i = d(\vec{P}_i, \vec{P}_{i+1})/d(\vec{P}_i, \vec{P}_{i-1})$ current ratio of distances;

d = geometric distance.

For each time offset value which is an integer multiple of a second and possible combination that corresponds to the same length of camera centers vector gives a curve of successive distances ratios of GPS positions which is compared to that of cameras centers. The ratios are used because both the GPS absolute and the photogrammetric relative frames do not have the same geometric scale. The combination of an offset value which gives the maximum value of the correlation coefficient between the two curves gives the corresponding GPS positions to the cameras centers. This method can be described as follows:

Algorithm 1. Matching GPS positions and Camera centers

```
input  : GPS positions & Camera centers
output: Corresponding positions ⇔ centers
Compute(dcr = distances cameras ratios);
Compute(nbrMaxTO = maximum number of possible time offsets);
for i ← 1 to nbrMaxTO do
    Compute(nbrMaxComb = maximum number of GPS trajectory
    combinaison);
    for j ← 1 to nbrMaxComb do
        get(corresponding current GPS positions);
        Compute(djr_j = distances Gps ratios);
        Compute(c(i, j) = corr(dcr, djr_j));
    end
end
Compute(max(c));
```

Fig. 6 illustrates the results of this method for a real dataset and gives results of maximum correlation coefficient for 3 values of time offset.

Values for all possible time offset between GPS positions and cameras centers and a time offset combination gives the maximum possible value for the correlation coefficient between the curves of distances ratios. The greater the time offset between the two sensors is, the lower the number of combinations to be tested will be. This method has been tested on multiple datasets and a unique combination gives the maximum value of the correlation coefficient. This method qualifies the consistency between the relative displacements measured by each sensor and allows to match the measurements.

4.4. Lever-arm calibration

To achieve precise direct sensor orientation, it is essential to consider the vector between the optical center of the camera and the phase center of the GPS antenna. There are several techniques to determine this vector. In a static way: the drone is positioned over a scene that contains georeferenced targets. This technique enables a static GPS processing, therefore a more accurate GPS positioning but requires a considerable time of acquisition (each image may require several hours of GPS carrier-phase observations). The 2nd method consists in a 3D modeling of the UAV before take-off with the sensors mounted with their centers (optical and antenna phase) previously calibrated according to materialized targets on the sensors. This technique has the advantage of always being valid even if relative positions of the sensors change from one acquisition to another, this last method is an instrumental calibration method performed by photogrammetric measurements (Daakir et al., 2016). The last method is the most conventional and commonly used. A calibration flight over a scene that contains georeferenced targets is performed (Daakir et al., 2015). Data processing is performed in kinematic mode. We will detail here only the second procedure via a calibration flight example.

Once the camera poses are estimated, GPS trajectory is processed and the GPS positions corresponding to images centers are extracted, it remains to estimate, at least, 10 parameters to achieve the georeferencing of the acquisition, assuming that the time synchronization is perfect. Out of these 10 parameters, 7 correspond to the spatial 3D similarity and the remaining 3 to the axial components of the lever-arm vector. The system of equations to minimize can be written for an image k as follows:

$$\begin{cases} \cdots\cdots \\ \vec{\mathcal{G}_k}|_t - \mu \cdot \mathcal{R} \cdot \vec{\mathcal{C}_k}|_r - \vec{\mathcal{T}} - \mathcal{R} \cdot \mathcal{R}_k^T \cdot \vec{\mathcal{O}} = \vec{0} \\ \cdots\cdots \end{cases} \quad (6)$$

where

$\vec{\mathcal{G}_k}|_t$ = GPS position of image k expressed in absolute frame;

μ = scaling factor;

$\mathcal{R}$ = global rotation;

$\vec{\mathcal{C}_k}|_r$ = image k center expressed in relative frame;

$\vec{\mathcal{T}}$ = global translation;

$\mathcal{R}_k$ = image k orientation;

$\vec{\mathcal{O}}$ = lever-arm vector.

In close-range photogrammetry aerial configuration, the orientation of the camera remains almost identical during the flight. The UAV autopilot system tends to stabilize at horizontal, which gives images a constant attitude. It is possible to solve the

[8] TOW: Time Of Week and epoch of GPS observations.

[9] This means that the chronological order is respected using for example images names.

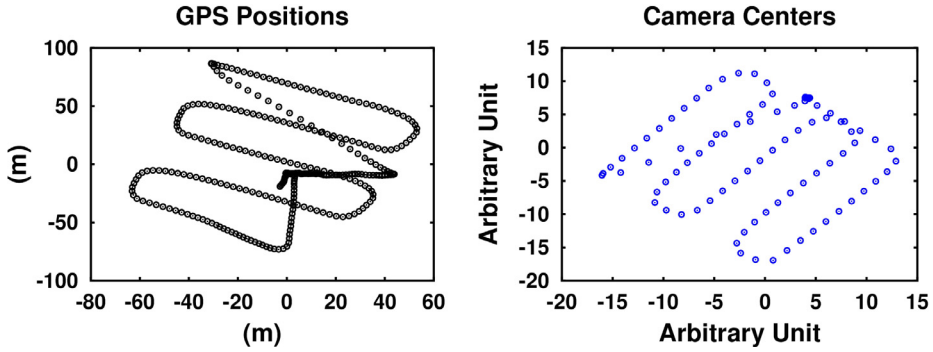

Fig. 5. Trajectories in different frames with different sampling.

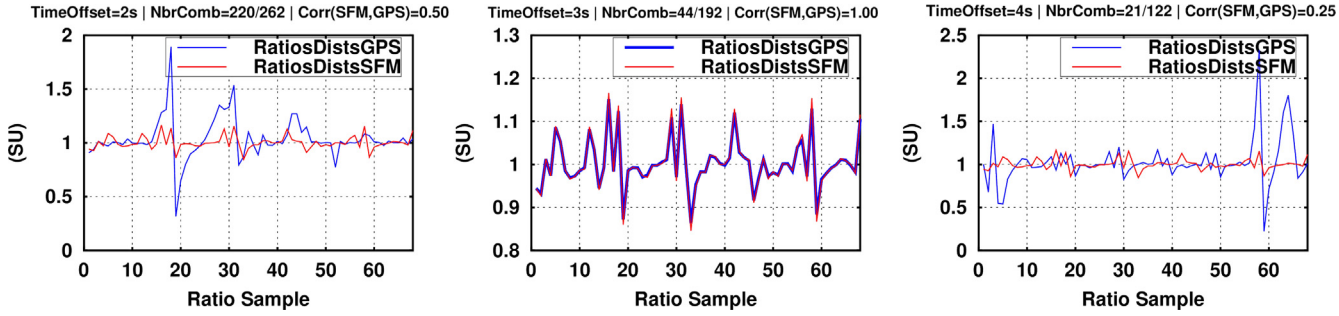

Fig. 6. Correlation values between ratios distances curves after testing different temporal offset values.

system of Eqs. (6) relying only on GPS data. However, this configuration of acquisition introduces a strong correlation between the parameter of global translation $\vec{\mathcal{T}}$ and the parameter of lever-arm $\vec{\mathcal{O}}$. This ambiguity can be resolved by introducing at least one external measurement. A ground control point equation should be added and the system to minimize can be written as follows:

$$\begin{cases} \cdots\cdots \\ \mathcal{G}_k^{\rightarrow}|_t - \mu \cdot \mathcal{R} \cdot \mathcal{C}_k^{\rightarrow}|_r - \mathcal{T}^{\rightarrow} - \mathcal{R} \cdot \mathcal{R}_k^T \cdot \mathcal{O}^{\rightarrow} = 0^{\rightarrow} \\ \cdots\cdots \\ \mathcal{P}_i^{\rightarrow}|_t - \mu \cdot \mathcal{R} \cdot \mathcal{P}_i^{\rightarrow}|_r - \mathcal{T}^{\rightarrow} = 0^{\rightarrow} \\ \cdots\cdots \end{cases} \tag{7}$$

where

$\vec{\mathcal{P}_i}|_t$ = ground control point expressed in absolute frame;

$\vec{\mathcal{P}_i}|_r$ = ground control point expressed in relative frame.

The equations concerning ground control points behave as constraint equations during the minimization. To illustrate, a calibration data set with 17 ground control points is used and is described in Section 5. Fig. 7 shows the variation of the lever-arm estimated value according to the number of ground control points used during the minimization.

The variation of the estimated value is large, in the order of 6 cm from a ground control point is introduced. The curves converge increasing the number of ground control points used. Beyond 5 points, the variation of the estimate value is at millimeter level.

4.5. Time synchronisation

4.5.1. Problem presentation

The guarantee of the same time-scale is crucial when using different data sources. Time synchronization between GPS measurements and images taken by the camera can be neglected if we have for example, a high sampling of GPS data which allows the use of interpolation techniques. To achieve the best time synchronization, we opted for a camera-triggering controlled by a GPS. *U-blox TimePulse* signal functionality provides clock pulses with configurable duration.The constraint of this feature is that the interval between pulses must always be an integer multiple so that the pulse is aligned with the TOW.

During our first experiments the camera chosen was the *Sony-RX1* model. Although this camera is not the one used in the following experiments, we present the synchronization aspect using a commercial camera. We show that this type of cameras is not adapted to perform sensors synchronization, although it is possible to correct this error by modifying the model that links observations. The *Sony-RX1* is a professional full-frame 24 Mpx compact camera. The lens is a fixed focal of 35 mm length. The optical quality of this lens is very honourable making the *Sony-RX1* a good commercial photogrammetric camera. However, there are a few disadvantages: no interchangeable optical lens capability and the camera is quite heavy (482 g), which is not suitable for a small UAV with relatively little flight autonomy. This camera is not cheap as it costs about €2500. Thanks to *LOEMI* laboratory the *Sony-RX1* camera was customized to achieve GPS triggering (Fig. 8).

A first measurement of the electronic delay was achieved at the laboratory. The measurement was carried out with an oscilloscope that shows both the waveform of the two electrical signals from the GPS pulse that triggers the camera and the outbreak of the camera. Camera-trigging for *Sony-RX1* is considered perfectly synchronized with the flash carrier while the measurement is performed on the *CMOS* pin control for *IGN* light camera.

Fig. 9 reports the pattern of the two signals. The red[10] curve corresponds to the GPS pulse whose rising edge starts taking pictures

[10] For interpretation of color in Figs. 6, 10 and 12, the reader is referred to the web version of this article.

Please cite this article in press as: Daakir, M., et al. Lightweight UAV with on-board photogrammetry and single-frequency GPS positioning for metrology applications. ISPRS J. Photogram. Remote Sensing (2017), http://dx.doi.org/10.1016/j.isprsjprs.2016.12.007

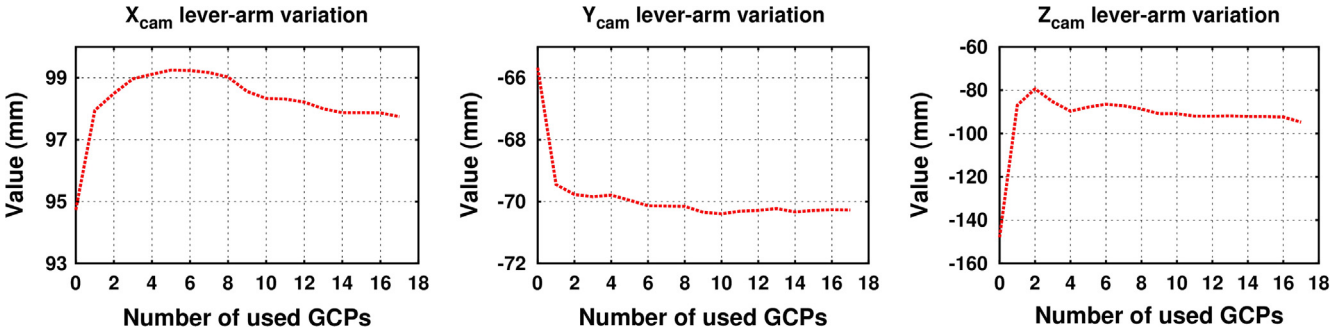

Fig. 7. Variation of lever-arm estimation value by number of used GCPs.

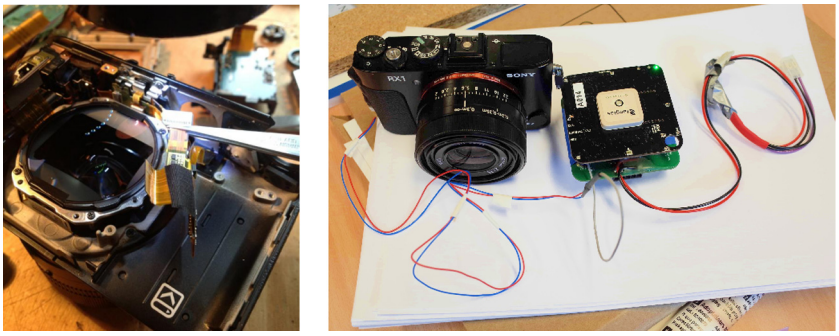

Fig. 8. Adapting *Sony-RX1* camera triggering with GPS module *TimePulse* feature.

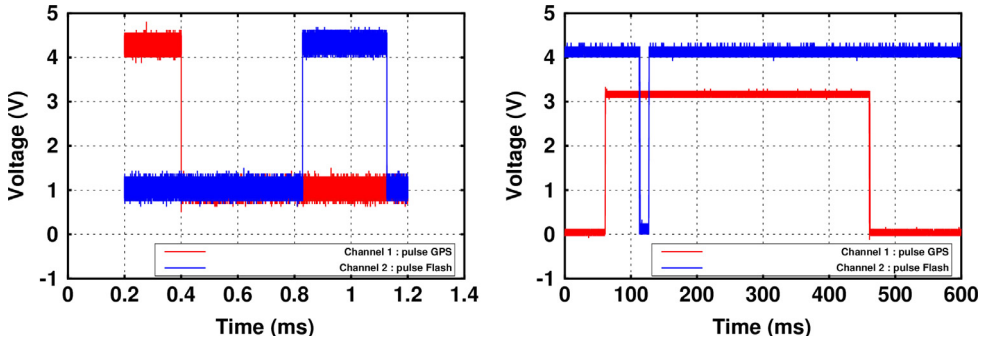

Fig. 9. Measurement of electronic delay with an oscilloscope: between GPS and *IGN* light camera (left) and *SONY-RX1* (right).

with a delay on the falling edge of the flash pulse of 0.4 ms for the first camera and 64 ms for the second one.

This measurement highlights the existence of an electronic delay between the two sensors, however, it does not prove that this value is steady over time and can be considered as a permanent constant bias. Given the complexity of the measurement using an oscilloscope another solution has allowed to describe the reproducibility of the electronic delay. The *TimeMark* functionality of the *u-blox* GPS module is used to date events in the GPS time-scale. Both cameras were adapted to recover the electronic pulse corresponding to the start of the exposure. Two events are dated: the *TimePulse* sent by the GPS to trigger the camera which is aligned to TOW and the *TimeMark* dated by the GPS which is the actual trigger of the camera. The difference in time between these two events is exactly the electronic delay and is equivalent to our measurement performed in the laboratory with an oscilloscope. Fig. 10 shows the reproducibility of the measurement of the delay.

For the camera manufactured internally the electronic delay value is very stable over time. For each triggering of the camera the value is less than 1 ms which represents a maximum error of 5 mm on the position at a typical UAV speed of 5 m/s. As for the *Sony-RX1* commercial camera, the value is unstable and changes over time, between 50 and 200 ms, which represents a maximum error of 1 m at the same speed.

In conclusion, even with the use of a high-end commercial camera, time synchronization remains a difficult problem to handle because standard cameras are not built to be used in this context. The development of a home-made UAV-metric camera provides solutions to this kind of problem. The current delay of ~ 0.4 ms managed by the software of the camera, has been improved to ~ 200 ns and managed by the hardware. The goal is to make it very negligible in any configuration of use of the camera (multi-rotors or fixed-wing UAVs).

4.5.2. Application

If it is impossible to achieve perfect time synchronization, for instance with the use of a commercial camera, and if the sampling of the GPS trajectory is not dense enough, it is possible to correct the electronic delay if measurements of instantaneous velocity of

Please cite this article in press as: Daakir, M., et al. Lightweight UAV with on-board photogrammetry and single-frequency GPS positioning for metrology applications. ISPRS J. Photogram. Remote Sensing (2017), http://dx.doi.org/10.1016/j.isprsjprs.2016.12.007

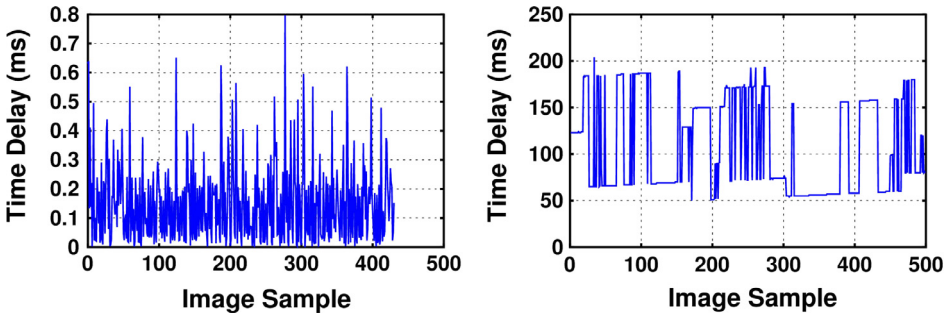

Fig. 10. Measurements of electronic delay stability with time difference pulses: *IGN* light camera (left) and *SONY-RX1* (right).

the UAV are available. In our case, the *u-blox* GPS receiver provides direct access to instantaneous velocities expressed in ECEF frame. If raw data of Doppler measurements are recorded by the GPS receiver it is possible to deduce instantaneous velocity values (Chalko, 2007). Hence a correction is added to system of Eq. (6) in both cases, delay is stable or variable and can be written as follows for an image k:

$$\begin{cases} \cdots\cdots \\ \mathcal{G}_k{}^{\rightarrow}|_t - \mathcal{S}(\mathcal{C}_k{}^{\rightarrow}|_r) - \mathcal{R}\cdot\mathcal{R}_k^T\cdot\mathcal{O}^{\rightarrow} - \mathcal{V}_k{}^{\rightarrow}|_t\cdot t_d = 0^{\rightarrow} \\ \qquad || \\ \mathcal{G}_k{}^{\rightarrow}|_t - \mathcal{S}(\mathcal{C}_k{}^{\rightarrow}|_r) - \mathcal{R}\cdot\mathcal{R}_k^T\cdot\mathcal{O}^{\rightarrow} - \mathcal{V}_k{}^{\rightarrow}|_t\cdot t_d^k = 0^{\rightarrow} \\ \cdots\cdots \end{cases} \tag{8}$$

where

$\mathcal{S}$ = 3D similarity application;
$\vec{\mathcal{V}}_k$ = instantaneous velocity of image k in absolute frame;
t_d = time delay parameter;
t_d^k = time delay parameter for image k.

An acquisition was performed using the *Sony-RX1* camera. This acquisition has 231 images and 10 ground control points. Images were acquired at a rate of 2 s. All ground control points were used to estimate parameters of system of Eqs. (7) and (8). Fig. 11 shows the residuals of the estimation assuming no electronic delay (10 parameters estimated) and variable delay (242 parameters estimated).

Taking electronic delay into account as shown by the measurements in Fig. 10 improves the relative accuracy between the two sensors by a factor of 12 for planimetric components and by a factor of 4 for the vertical component. This error in the position largely impacts the planimetric axial components. Indeed, the autopilot system allows the UAV to maintain a constant flight height based on a barometric sensor that makes vertical speeds very low and reduces synchronization error for this component.

4.6. Data fusion

An essential step to optimize the final accuracy of georeferencing process is to refine all parameters using all available observations in a bundle adjustment. The observations which can be used are tie points, GPS camera positions and, optionally, at least one ground control point if the lever-arm vector is unknown. This involves an estimate for N images of an acquisition, at least, $(6\cdot N+10)$ unknown parameters of the observation system assuming that the internal camera parameters are determined beforehand. *Apero-MicMac* photogrammetric suite also offers the

Fig. 11. Comparison of residuals with and without taking delay into account. Planimetric components (left and center) and vertical component (right).

Please cite this article in press as: Daakir, M., et al. Lightweight UAV with on-board photogrammetry and single-frequency GPS positioning for metrology applications. ISPRS J. Photogram. Remote Sensing (2017), http://dx.doi.org/10.1016/j.isprsjprs.2016.12.007

Table 1
Residuals on check points depending on processing strategies.

	Estimated parameters				MAE[a] (cm/px)	s[b] (cm)
	Relative poses	Absolute centers	Lever-arm	Camera model		
$\mathcal{S}_1$	(Section 4.1)	(Section 4.2)	(Section 4.4)	(Section 4.1)	2.4/2.0	0.8
$\mathcal{S}_2$	Tightly coupled		–	–	0.8/0.7	0.8
$\mathcal{S}_3$	Tightly coupled			–	0.8/0.7	0.8
$\mathcal{S}_4$	Tightly coupled		–	Tightly coupled	0.8/0.7	0.7
$\mathcal{S}_5$	Tightly coupled				0.8/0.7	0.8

[a] Mean Absolute Error.
[b] Standard Deviation.

opportunity to refine simultaneously the internal parameters of the camera which can improve the accuracy in case of a self-calibration bundle block adjustment based only on tie points.

The same dataset of calibration flight in part (Section 4.4) is used. 5 points are used as ground control points to calibrate the lever-arm vector, while the remaining 12 points are used as control measurements in order to qualify georeferencing accuracy. Table 1 provides statistical indicators of the gain in accuracy with the global compensation technique, assuming different strategies $[\![\mathcal{S}_1 : \mathcal{S}_5]\!]$.

Strategy $\mathcal{S}_1$ is a camera poses conversion from relative into absolute frame by estimating 10 parameters of the system of Eq. (7). Strategy $\mathcal{S}_2$ is a minimization of system of Eqs. (7) and (1) through a bundle block adjustment where heterogeneous observations (tie points, GPS positions and GCPs) are used simultaneously. The parameters estimated here are the parameters of 3D similarity and the position and orientation of each image. Strategy $\mathcal{S}_3$ introduces the lever-arm as a parameter to refine in the global compensation. Strategy $\mathcal{S}_4$ fixes the lever-arm while the camera model ζ of system of Eq. (7) is introduced as a parameter to refine. Strategy $\mathcal{S}_5 = \{\mathcal{S}_3 \cup \mathcal{S}_4\}$.

The lower residual obtained on check points is found by performing a global compensation with free internal parameters. However, the difference is very low when compared to a global compensation where only exterior parameters are estimated again. This is a good indicator that the estimation of internal parameters by self-calibration gives a correct result using the strategy presented in Section 4.1 for this dataset. For the third strategy, estimating again the lever-arm value gives a variation of 3 mm in the norm of the vector that has a value of 15.0 cm. The last combination is a degenerate combination where the accuracy is still equivalent to other strategies but where the focal length and lever-arm estimation are wrong. In fact here, the variation of the lever-arm value is 7.4 cm and it impacts the vertical component by 95%. This variation is compensated by a variation of 7 pixels of the focal length estimation, which still gives correct residuals on check points but incorrect parameter estimation. Indeed, in this configuration, the correlation between the focal length and the vertical component of the lever-arm vector makes the estimation of these two unknown parameters ambiguous.

In order to compare these different processing strategies standard deviations of the estimated parameters can be discussed. Table 2 gives, for strategies with similar results ($\mathcal{S}_2$ to $\mathcal{S}_5$), the mean value of estimated standard deviation for external parameters, lever-arm vector, focal length and principal point. This table confirms that the $\mathcal{S}_5$ strategy gives an estimate with high uncertainty on the focal length (0.75 px) and the lever-arm offset (0.041 m), while the strategy that gives the lowest uncertainties is the $\mathcal{S}_4$ strategy. The final strategy adopted for data fusion of heterogeneous observations is the following: two successive compensations are performed to avoid degenerate configuration where the focal length is correlated with the vertical component of the lever-arm vector. Indeed, a first compensation is achieved by releasing the lever-arm to refine its estimate ($\mathcal{S}_3$), then the result is used as an input for a second compensation where, this time, the internal camera parameters are released to refine their estimates using not only tie points, but also external ground control points measurements ($\mathcal{S}_4$).

5. Experimental survey

This part will show the results of 2 UAV flights performed with the same system presented in Section 3. The first flight is considered as a calibration flight and the second one is a flight used to qualify the repeatability of calibration parameters. The same flight plan is used to perform both flights based on *DJI Ground Station* software. (Fig. 12 left) shows a screen-shot of the achieved flight plan. The flying height was set at 70 m for a GSD of 1 cm. Overlap parameters are 75–35% and the surface covered is about 2 ha. Both flights are composed of a hundred images. The duration of each flight is less than 15 min. The scene has 17 ground control points whose coordinates were measured using a GPS RTK[11] system.

The two images in (Fig. 12 center and right) show the acquired images and the geometry of the acquisition after performing a bundle block adjustment following the strategy presented in Section 4.1. The panchromatic version of the camera is used. Camera centers are represented in green and red, GPS positions in blue, ground control points in yellow and check point in red.

5.1. Calibration flight

The first flight is used to calibrate all assumed parameters, constant from one acquisition to another, namely, internal parameters of the camera as well as lever-arm vector. It is assumed that the relative mounting of the sensors on the UAV is the same. Relative poses estimation based only on tie points gives an average residual of 0.26 px with more than 99% of extracted tie points used in the bundle. For this configuration electronic delay is considered as negligible. Table 3 gives residuals in available check points after parameters estimation using 5 ground control points used as a constraint for lever-arm estimation:

The accuracy[12] of the calibration procedure is estimated at 2σ level to: $\mu = 0.8 \pm 0.5$ cm.

5.2. Second flight

The second flight is used, based on the previous calibration parameters, to evaluate the accuracy of the predictive ability of our system. The internal parameters and the lever-arm vector estimated during the previous flight (Section 5.1) will be forced during data processing. The accuracy of georeferencing is evaluated through residuals in all available check points. Relative poses estimation based only on tie points, with the camera internal

[11] Real Time Kinematics.
[12] $\mu = \bar{x} \pm t \cdot \frac{s}{\sqrt{n}}$ where: $\bar{x} = ||\bar{\delta}_x^2 + \bar{\delta}_y^2 + \bar{\delta}_z^2||$, t = Student coefficient and n = size of sample.

Please cite this article in press as: Daakir, M., et al. Lightweight UAV with on-board photogrammetry and single-frequency GPS positioning for metrology applications. ISPRS J. Photogram. Remote Sensing (2017), http://dx.doi.org/10.1016/j.isprsjprs.2016.12.007

Table 2
Standard deviations of parameters for different strategies.

	$\mathcal{S}_2$	$\mathcal{S}_3$	$\mathcal{S}_4$	$\mathcal{S}_5$
$\bar{\sigma}_{C_x}$ (m)	0.003	0.005	0.003	0.005
$\bar{\sigma}_{C_y}$ (m)	0.002	0.004	0.002	0.003
$\bar{\sigma}_{C_z}$ (m)	0.001	0.003	0.001	0.004
$\bar{\sigma}_{C_\omega}$ (°)	0.001	0.001	0.001	0.001
$\bar{\sigma}_{C_\phi}$ (°)	0.001	0.004	0.001	0.004
$\bar{\sigma}_{C_\kappa}$ (°)	0.001	0.003	0.001	0.003
σ_{O_x} (m)	–	0.002	–	0.003
σ_{O_y} (m)	–	0.001	–	0.003
σ_{O_z} (m)	–	0.004	–	0.041
σ_f (px)	–	–	0.27	0.75
σ_{PP_x} (px)	–	–	0.34	0.37
σ_{PP_y} (px)	–	–	0.35	0.39

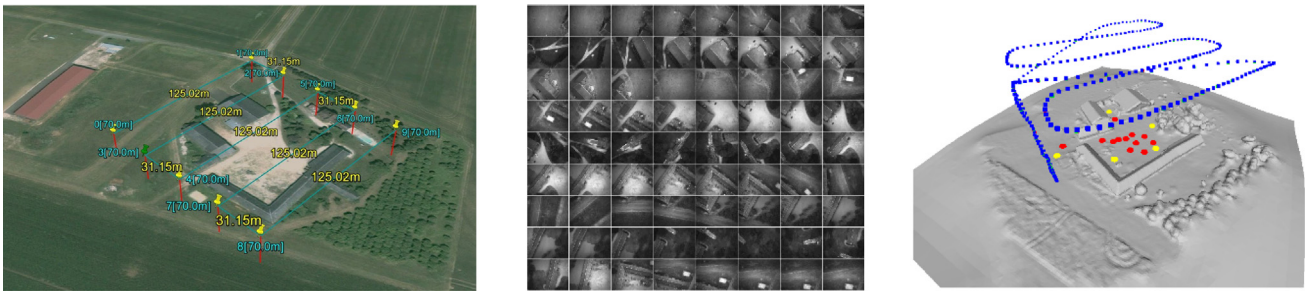

Fig. 12. Flight plan (left), panel of images (center) and acquisition geometry (right).

Table 3
Residuals on check points for flight calibration parameters.

Nom Pt	δx (cm)	δy (cm)	δz (cm)	$\|\|\delta\|\|$ (cm)
Pt_1	−0.2	0.8	−0.3	0.9
Pt_2	0.2	0.5	0.4	0.6
Pt_3	0.4	0.3	0.3	0.6
Pt_4	−0.1	0.4	0.5	0.7
Pt_5	0.5	0.6	0.1	0.8
Pt_6	−0.5	1.0	1.5	1.9
Pt_7	−0.1	0.5	−0.2	0.6
Pt_8	0.0	0.4	1.6	1.6
Pt_9	0.0	0.1	1.8	1.8
Pt_{10}	0.0	0.1	0.3	0.3
Pt_{11}	−0.2	0.5	0.3	0.7
Pt_{12}	−0.1	−0.1	−0.2	0.2
MAE	0.2	0.5	0.6	0.8
s	0.3	0.3	0.7	0.8

parameters frozen, gives an average residual of 0.30 px with 98% of extracted tie points used in the bundle. Table 4 shows residuals in available check points after correction of GPS estimated positions of lever-arm calibrated value.

The accuracy performed by our coupled system after performing a flight calibration is estimated at 2σ level to: $\mu = 2.0 \pm 0.5$ cm. Adding GCPs in the global compensation reduce the residuals on check points. For example, with the use of 1 GCP, the accuracy improves to 1.7 cm $\pm$ 0.4 cm while using 3 GCPs gives an accuracy of 1.0 cm $\pm$ 0.4.

5.3. GCPs Vs GPS

Quality control of final products is essential. In fact, the delivered results are orthoimage and computed DSM[13] expressed as a 3D point cloud. Check points allow us to control the accuracy of the georeferencing of camera poses but not of the DSM calculated.

A conversion of relative cameras poses into absolute ones using all available ground measurements is performed. This set of orientations is considered as a reference parameters set. One of the techniques used to control the quality of the final product is to generate a dense reference point cloud which will be compared to point cloud produced by a GPS integrated sensor orientation of camera poses. To perform this step the module *MicMac* (Pierrot-Deseilligny and Paparoditis, 2006), based on a multi-scale and multi-resolution approach is used to generate DSMs keeping the same parameters. Two point clouds are then compared, one generated with cameras poses georeferenced based only on the embedded GPS data and the second one generated using cameras poses georeferenced using all check points, computing Cloud-to-Mesh distances. This comparison is performed using *CloudCompare* (CloudCompare, 2016), a free open-source software for 3*D* point cloud and mesh processing. Fig. 13 shows the result of the comparison between the two generated point clouds.

[13] Digital Surface Model.

Please cite this article in press as: Daakir, M., et al. Lightweight UAV with on-board photogrammetry and single-frequency GPS positioning for metrology applications. ISPRS J. Photogram. Remote Sensing (2017), http://dx.doi.org/10.1016/j.isprsjprs.2016.12.007

Table 4
Residuals on check points for second flight.

Nom Pt	δx (cm)	δy (cm)	δz (cm)	$\|\|\delta\|\|$ (cm)
Pt_1	−0.7	0.3	−2.1	2.2
Pt_2	−1.4	−0.7	−1.7	2.3
Pt_3	−1.8	−0.2	−2.3	2.9
Pt_4	−1.1	−0.7	−1.1	1.7
Pt_5	−1.2	−0.4	−1.8	2.1
Pt_6	−1.0	−0.6	−1.7	2.1
Pt_7	−1.5	−0.2	−1.4	2.0
Pt_8	−1.0	−0.1	−1.7	2.0
Pt_9	−1.8	−1.7	−2.3	3.4
Pt_{10}	−1.1	−0.1	−0.2	1.1
Pt_{11}	−1.0	0.4	−1.1	1.6
Pt_{12}	−1.0	0.6	−1.3	1.7
Pt_{13}	−1.5	0.0	−0.6	1.6
Pt_{14}	−1.6	−0.4	−0.4	1.7
Pt_{15}	−1.7	−0.2	−1.1	2.1
Pt_{16}	−1.8	−0.1	−1.6	2.4
Pt_{17}	−2.0	−0.7	−1.9	2.8
MAE	1.4	0.4	1.4	2.0
s	0.4	0.5	0.6	0.9

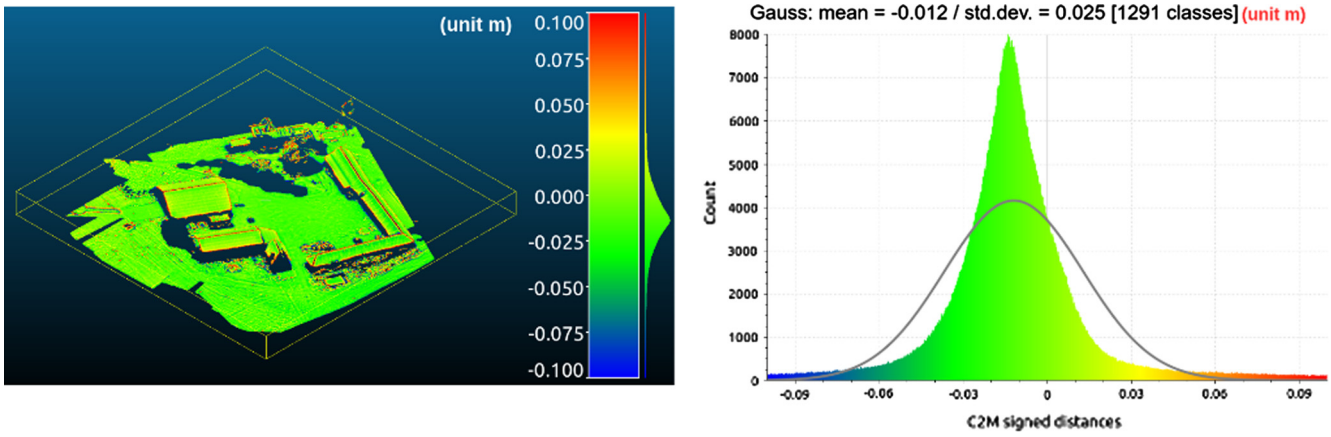

Fig. 13. Comparison between both point clouds using *CloudCompare*.

The result of the comparison gives a mean signed difference of 1.2 cm with a dispersion of 2.5 cm. The tendency is relatively of the same order of size as the control carried out on the quality of cameras poses georeferencing. Point clouds comparison control is subject to matching errors, however, for many applications, mostly in earthworks, which is our case, the challenge is to identify the existence of potential bias on large surfaces. In general the quality control of cameras poses based on check points is a robust indicator of the quality of absolute performed georeferencing.

6. Conclusion

In this article we show that it is possible to perform direct sensor orientation of acquired images of a photogrammetric quality camera mounted on a UAV based only on a single-frequency GPS module. The hardware integration was performed in the laboratory, building home-made instruments based on available market sensors. This part in particular has allowed us to control the geometric calibration aspect of our sensors as well as the time synchronization issue with our instruments. The system developed has also the singularity of being lightweight (2 kg) which makes it easy to transport. The accuracy achieved by our system is 2 cm ± 0.5 cm using 0 GCP based on calibration parameters (lever-arm offset and camera internal parameters) calculated on a first acquisition. The accuracy achieved using 1 GCP is 1.7 cm ± 0.4 cm while increasing the number of GCPs to 3 points gives an accuracy of 1.0 cm ± 0.4. These accuracies values reached by our system show that it meets the tolerances imposed in many mapping areas and makes it suitable to produce 3D models for metrological measurements applications where traditional techniques of surveying take time. In future work, the stability of the system, particularly the stability of the internal parameters of the camera will be investigated, while the lever-arm offset can be estimated robustly by adapting the flight plan. If the camera has a proper reproducibility it is possible to use this system with 0 GCP although it is always advisable to have at least 1 GCP to improve final accuracy.

7. Further work

The system developed in this study shows that it is possible to achieve centimeter absolute accuracy using low-cost sensors whose development and integration were performed in a laboratory. Future work will carry on, with the aim of improving accuracy, for example by testing the addition of a second frequency GPS data. This is why, nowadays, the significant development of OEM[14] for embedded systems drives manufacturers to offer cheap dual-frequency GNSS models.

[14] Original Equipment Manufacturer.

Please cite this article in press as: Daakir, M., et al. Lightweight UAV with on-board photogrammetry and single-frequency GPS positioning for metrology applications. ISPRS J. Photogram. Remote Sensing (2017), http://dx.doi.org/10.1016/j.isprsjprs.2016.12.007

Acknowledgements

We would like to thank *Vinci-Construction-Terrassement* for funding this research, *IGN* for hosting and supervising it, *LOEMI* laboratory for all its hardware support.

References

Bendea, H., Boccardo, P., Dequal, S., Giulio Tonolo, F., Marenchino, D., Piras, M., 2008. Low cost UAV for post-disaster assessment. ISPRS – Int. Arch. Photogram., Rem. Sens. Spatial Inform. Sci. 37 (Part B), 1373–1379.

Benoit, L., 2014. Positionnement GPS précis et en temps-réel dans le contexte de réseaux de capteurs sans fil type Geocube: application à des objets géophysiques de taille kilométrique PhD thesis. École Normale Supérieure.

Benoit, L., Briole, P., Martin, O., Thom, C., Malet, J.-P., Ulrich, P., 2015. Monitoring landslide displacements with the Geocube wireless network of low-cost GPS. Eng. Geol. 195, 111–121.

Bláha, M., Eisenbeiss, H., Grimm, D., Limpach, P., 2011. Direct georeferencing of UAVS. ISPRS – Int. Arch. Photogram., Rem. Sens. Spatial Inform. Sci. XXXVIII-1/C22, 131–136.

Chalko, T.J., 2007. High accuracy speed measurement using GPS (Global Positioning System). NU J. Discov. 4, 1–9.

Chiang, K.-W., Tsai, M.-L., Chu, C.-H., 2012. The development of an UAV borne direct georeferenced photogrammetric platform for ground control point free applications. Sensors 12 (7), 9161.

CloudCompare (version 2.6.0) [GPL software], 2016. <http://www.cloudcompare.org/> (Accessed 03 August, 2016).

Colomina, I., Molina, P., 2014. Unmanned aerial systems for photogrammetry and remote sensing: a review. ISPRS J. Photogram. Rem. Sens. 92, 79–97.

Daakir, M., Pierrot-Deseilligny, M., Bosser, P., Pichard, F., Thom, C., 2015. UAV onboard photogrammetry and GPS positionning for earthworks. ISPRS – Int. Arch. Photogram., Rem. Sens. Spatial Inform. Sci. XL-3/W3, 293–298.

Daakir, M., Pierrot-Deseilligny, M., Bosser, P., Pichard, F., Thom, C., Rabot, Y., 2016. Study of lever-arm effect using embedded photogrammetry and on-board GPS receiver on UAV for metrological mapping purpose and proposal of a free ground measurements calibration procedure. ISPRS – Int. Arch. Photogramm., Rem. Sens. Spatial Inform. Sci. XL-3/W4, 65–70.

DJI Innovations, 2014. WooKong-M Quick Start Guide. <http://dl.djicdn.com/downloads/wkm/en/WooKong-M_Quick_Start_Guide_v1.14_en.pdf> (Accessed 03 August, 2016).

DJI Innovations, 2015a. FlameWheel 550 User Manual. <http://dl.djicdn.com/downloads/flamewheel/en/F550_User_Manual_v2.0_en.pdf> (Accessed 03 August, 2016).

DJI Innovations, 2015b. Ground Station Wireless Data-link User Manual. <http://dl.djicdn.com/downloads/groundstation/en/Ground_Station_User_Manual_en_v3.04.pdf> (Accessed 03 August, 2016).

Eisenbeiß, H., 2004. A mini unmanned aerial vehicle (UAV): system overview and image acquisition. Int. Arch. Photogram. Rem. Sens. Spatial Inform. Sci. 36 (5/W1).

Eisenbeiß, H., 2009. UAV Photogrammetry PhD Thesis. Institut für Geodesie und Photogrammetrie, ETH-Zürich. Zürich, Switzerland.

Eling, C., Klingbeil, L., Kuhlmann, H., 2015. Real-time single-frequency GPS/MEMS-IMU attitude determination of lightweight UAVS. Sensors 15 (10), 26212–26235.

Fraser, C.S., 1997. Digital camera self-calibration. ISPRS J. Photogram. Rem. Sens. 52 (4), 149–159.

Grenzdörffer, G., Engel, A., Teichert, B., 2008. The photogrammetric potential of low-cost UAVs in forestry and agriculture. Int. Arch. Photogram., Rem. Sens. Spatial Inform. Sci. 31 (B3), 1207–1214.

James, M.R., Robson, S., 2014. Mitigating systematic error in topographic models derived from UAV and ground-based image networks. Earth Surf. Process. Landforms 39 (10), 1413–1420.

Klobuchar, J.A., 1987. Ionospheric time-delay algorithm for single-frequency GPS users. IEEE Trans. Aerospace Electron. Syst. AES-23 (3), 325–331.

Lisein, J., Pierrot-Deseilligny, M., Bonnet, S., Lejeune, P., 2013. A photogrammetric workflow for the creation of a forest canopy height model from small unmanned aerial system imagery. Forests 4 (4), 922–944.

Lowe, D.G., 2004. Distinctive image features from scale-invariant keypoints. Int. J. Comput. Vis. 60 (2), 91–110.

Martin, O., Meynard, C., Pierrot-Deseilligny, M., Souchon, J., Thom, C., 2014. Réalisation d'une caméra photogrammétrique ultralégère et de haute résolution. <https://drone.teledetection.fr/articles/Souchon_CAMLIGHT_IGN_rev.pdf> (Accessed 07 December, 2016).

Niethammer, U., James, M., Rothmund, S., Travelletti, J., Joswig, M., 2012. UAV-based remote sensing of the Super-Sauze landslide: evaluation and results. Eng. Geol. 128, 2–11 (Integration of Technologies for Landslide Monitoring and Quantitative Hazard Assessment).

Pierrot-Deseilligny, M., 2017. MicMac, Apero, Pastis and Other Beverages in a Nutshell! <https://github.com/micmacIGN/Documentation/blob/master/DocMicMac.pdf> (Accessed 10 February, 2017).

Pierrot-Deseilligny, M., Clery Apero, I., 2011. An open source bundle adjustment software for automatic calibration and orientation of set of images. ISPRS – Int. Arch. Photogram., Rem. Sens. Spatial Inform. Sci. XXXVIII-5/W16, 269–276.

Pierrot-Deseilligny, M., Paparoditis, N., 2006. A multiresolution and optimization-based image matching approach: an application to surface reconstruction from spot 5-h stereo imagery. Arch. Photogram., Rem. Sens. Spatial Inform. Sci. 36 (1/W41).

Rehak, M., Mabillard, R., Skaloud, J., 2013. A micro-UAV with the capability of direct georeferencing. ISPRS – Int. Arch. Photogram., Rem. Sens. Spatial Inform. Sci. XL-1/W2, 317–323.

Remondino, F., Barazzetti, L., Nex, F., Scaioni, M., Sarazzi, D., 2011. UAV photogrammetry for mapping and 3d modeling–current status and future perspectives. Int. Arch. Photogram., Rem. Sens. Spatial Inform. Sci. 38 (1), C22.

Rieke, M., Foerster, T., Geipel, J., Prinz, T., 2011. High-precision positioning and real-time data processing of UAV-systems. Int. Arch. Photogram., Rem. Sens. Spatial Inform. Sci. 38, 1–C22.

Saastamoinen, J., 1972. Atmospheric correction for the troposphere and stratosphere in radio ranging satellites. The Use Artif. Satel. Geodesy, 247–251.

Skaloud, J., 2002. Direct georeferencing in aerial photogrammetric mapping. Photogram. Eng. Rem. Sens. 68 (3).

Stempfhuber, W., Buchholz, M., 2011. A precise, low-cost RTK GNSS system for UAV applications. ISPRS – Int. Arch. Photogram., Rem. Sens. Spatial Inform. Sci. XXXVIII-1/C22, 289–293.

Tang, R., 2013. Mathematical Methods for Camera Self-calibration in Photogrammetry and Computer Vision PhD Thesis. University of Stuttgart.

Tournadre, V., Pierrot-Deseilligny, M., Faure, P.H., 2014. UAV photogrammetry to monitor dykes – calibration and comparison to terrestrial LIDAR. ISPRS – Int. Arch. Photogram., Rem. Sens. Spatial Inform. Sci. XL-3/W1, 143–148.

Tournadre, V., Pierrot-Deseilligny, M., Faure, P.H., 2015. UAV linear photogrammetry. ISPRS – Int. Arch. Photogram., Rem. Sens. Spatial Inform. Sci. XL-3/W3, 327–333.

Triggs, B., McLauchlan, P.F., Hartley, R.I., Fitzgibbon, A.W., 1999. Bundle adjustment – a modern synthesis. In: International Workshop on Vision Algorithms. Springer, pp. 298–372.

u-blox (2013). u-blox 6 Receiver Description Including Protocol Specification. <https://www.u-blox.com/sites/default/files/products/documents/u-blox6_ReceiverDescrProtSpec_%28GPS.G6-SW-10018%29_Public.pdf?utm_source=en%2Fimages%2Fdownloads%2FProduct_Docs%2Fu-blox6_ReceiverDescriptionProtocolSpec_%28GPS.G6-SW-10018%29.pdf> (Accessed 03 August, 2016).

u-blox (2015). LEA-6 u-blox 6 GPS Modules Data Sheet Objective Specification. <https://www.u-blox.com/sites/default/files/products/documents/LEA-6_DataSheet_(UBX-14044797).pdf> (Accessed 03 August, 2016).

u-blox (2016). u-center GNSS evaluation software for Windows User Guide. <https://www.u-blox.com/sites/default/files/u-Center_UserGuide_(UBX-13005250).pdf> (Accessed 03 August, 2016).

Wu, C., 2014. Critical configurations for radial distortion self-calibration. In: Proceedings of the IEEE Conference on Computer Vision and Pattern Recognition, pp. 25–32.

Please cite this article in press as: Daakir, M., et al. Lightweight UAV with on-board photogrammetry and single-frequency GPS positioning for metrology applications. ISPRS J. Photogram. Remote Sensing (2017), http://dx.doi.org/10.1016/j.isprsjprs.2016.12.007